ACS SyntheticBiology

Research Article

pubs.acs.org/synthbio

Influence of Electrostatics on Small Molecule Flux through a Protein Nanoreactor

Jeff E. Glasgow,[†] Michael A. Asensio,[‡] Christopher M. Jakobson,[§] Matthew B. Francis,[†] and Danielle Tullman-Ercek*[,§]

[†]Department of Chemistry, [‡]Department of Bioengineering, [§]Department of Chemical and Biomolecular Engineering, University of California, Berkeley, California 94720, United States

Supporting Information

ABSTRACT: Nature uses protein compartmentalization to great effect for control over enzymatic pathways, and the strategy has great promise for synthetic biology. In particular, encapsulation in nanometer-sized containers to create nanoreactors has the potential to elicit interesting, unexplored effects resulting from deviations from well-understood bulk processes. Self-assembled protein shells for encapsulation are especially desirable for their uniform structures and ease of perturbation through genetic mutation. Here, we use the MS2 capsid, a well-defined porous 27 nm protein shell, as an enzymatic nanoreactor to explore pore-structure effects on substrate and product flux during the catalyzed reaction. Our results suggest that the shell can influence the enzymatic reaction based on charge repulsion between small molecules and point mutations around the pore structure. These findings also lend support to the hypothesis that protein compartments modulate the transport of small molecules and thus influence metabolic reactions and catalysis *in vitro*.

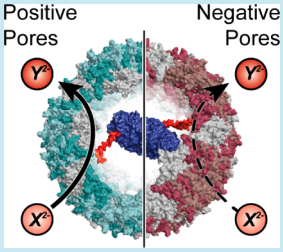

KEYWORDS: *compartmentalization, enzyme encapsulation, virus, enzyme catalysis, nanobioreactor*

Natural metabolic systems provide numerous examples of enzyme colocalization occurring through genetic fusion, direct binding interactions, scaffolding, or compartmentalization.[1−4] This is thought to facilitate pathway flux by increasing the local concentrations of intermediate molecules around downstream enzymes while limiting off-target reactions that can lead to unproductive accumulation or even toxicity.[5−8] Many researchers have attempted to recapitulate and use this effect *in vitro* and *in vivo* by adding artificial scaffolding,[9−13] localizing enzymes to specific organelles,[14,15] engineering the enzymes,[16−18] or encapsulating them in protein compartments[19−23] and polymersomes.[24−28] Despite numerous technological advances, one aspect of compartmentalization that has yet to be fully explored is the ability to influence the passive diffusion of substrates, products, and intermediates. Decreasing the diffusion of intermediates compared to substrates and products across the shell of an enzyme-containing compartment may be a method to enhance pathway flux without altering individual proteins.

Permeability effects were examined in a variety of inorganic and polymeric nanoreactors,[29−33] but only a handful of protein complexes have been studied for such properties. Ferritin cages, for example, direct Fe(II) ions for oxidation using negatively charged pores.[34] Natural membrane protein ion channels have both ion-specific and nonspecific electrostatic interactions with their substrates, affecting their transfer kinetics and selectivity.[35] The carboxysome, a protein-based bacterial microcompartment, is also hypothesized to use positively charged pores to allow passive diffusion of bicarbonate ions while retaining hydrophobic CO_2 and excluding molecular oxygen, which can lead to undesired side reactions.[36−38] Inspired by these natural systems, we sought to develop a protein-based nanoreactor with mutable pores to examine the effects of electrostatics on substrate and product flux (Figure 1). For this proof-of-concept study, we

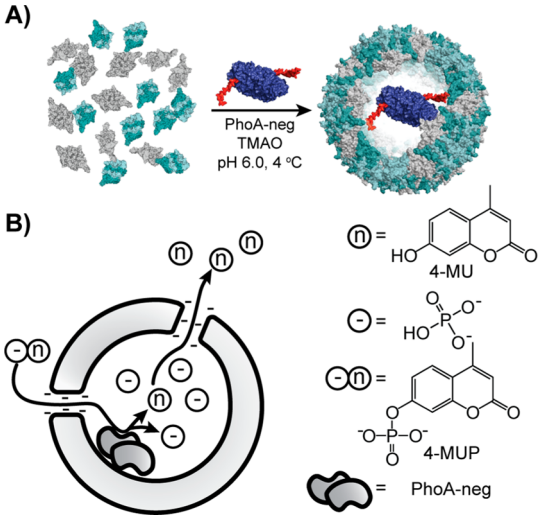

Figure 1. Testing the effects of pore charge on substrate and product flux. (A) Bacteriophage MS2-based enzymatic nanoreactors are created through self-assembly of the capsid around negatively charged alkaline phosphatase (PhoA-neg) variants. (B) Capsid pore charge is varied by mutagenesis, and reactions of negatively charged phosphatase substrates are monitored.

Received: February 22, 2015
Published: April 20, 2015

DOI: 10.1021/acssynbio.5b00037
ACS Synth. Biol. 2015, 4, 1011−1019

chose to analyze the effect on a single enzyme reaction, with the expectation that the approach can be expanded to multienzyme pathways in the future.

The bacteriophage MS2 forms an icosahedral capsid from 180 monomers that is 27 nm in diameter with triangulation number T = 3 and pores at its vertices. We previously developed the MS2 viral capsid as a stable, versatile compartment for encapsulation of negatively charged macromolecules enhanced by the presence of a protein-stabilizing osmolyte, trimethylamine-*N*-oxide (TMAO).[39,40] The capsid is also well-characterized for tolerance to mutations, particularly in the assembly directing pore residues of the FG-loop.[41,42] This loop forms the intersubunit contacts lining the 1.8 nm pores at the 5-fold and quasi-6-fold axes of the icosahedral capsid. Point mutations in this loop can thus add charge directly around the capsid pores, allowing controllable, genetically encoded modifications to the pore environment. Here, we show that capsids mutated in this way are able to encapsulate alkaline phosphatase enzymes bearing a localization tag. When these enzymes are inside capsids with pores having no charge or a charge opposite to that of the substrate, the apparent K_M ($K_{M,app}$) is similar to that of the free enzyme; however, when pore and substrate charge are the same, the $K_{M,app}$ of the enzyme increases significantly. Kinetic modeling suggests this could be caused primarily by reduced product efflux, leading to inhibition of the enzyme. These experiments represent a first step in creating selective nanoreactors with the potential either to protect cargo by inhibiting entrance of interfering molecules or to enhance multistep pathways by concentrating internal intermediates.

RESULTS AND DISCUSSION

Encapsulation of Alkaline Phosphatase in Mutated MS2 Capsids. We generated several mutants of the wild-type MS2 ($MS2^{WT}$) capsid by QuikChange mutagenesis and expressed them as described[39] (Supporting Information Table S1). The T71E ($MS2^{T71E}$) and T71E/V72D ($MS2^{T71E/V72D}$) mutations add one or two negative charges to each subunit, respectively, whereas the T71K/V72R ($MS2^{T71K/V72R}$) mutation adds two positive charges. This results in capsids with increased negative (in the case of $MS2^{T71E}$ and $MS2^{T71E/V72D}$) or positive (in the case of $MS2^{T71K/V72R}$) charge around the 5-fold and quasi-6-fold axis pores on each capsid. Figure 2 depicts one possible conformation of these residues and their predicted electrostatics. The mutations have little or no effect on expression and assembly in *Escherichia coli*, and they have only a small effect on the thermal stability of the capsids (Supporting Information Figures S1 and S2).

We subjected each of these mutants to our previously developed disassembly/reassembly protocol, which encapsulates negatively charged molecules, such as enzymes, based on electrostatic interactions with the positive residues on the capsid interior surface. To initiate reassembly, we used a model enzyme, *E. coli* alkaline phosphatase, with a C-terminal sequence of 16 negatively charged amino acids ($PhoA^{WT}$-neg).[39] The $MS2^{T71K/V72R}$ mutant reassembled similarly to the $MS2^{WT}$ capsid under these conditions (50 mM Tris HCl, pH 7.2, 100 mM NaCl, 36−48 h, 4 °C; Supporting Information Figure S1). The $MS2^{T71E}$ and $MS2^{T71E/V72D}$ mutants, however, gave significantly lower yields of reassembled product. We varied the salt, pH, and TMAO concentrations of the reassembly reaction to determine what conditions favored reassembly of these mutants. While salt concentration did not significantly affect the yield of reassembled capsid, lowering the pH from 7.2 to 6.0 and increasing the TMAO concentration from 0.25 to 1.8 M enhanced the yield of reassembled $MS2^{T71E}$ and $MS2^{T71E/V72D}$ capsids by 8-fold. Using these improved reassembly conditions, we obtained between 3 and 10 enzymes encapsulated per capsid in each of the MS2 mutants. The reassembly conditions did not affect the activity of the enzyme after purification (Supporting Information Figure S3). Subsequent enzyme assays were performed in identical buffers for each capsid mutant, as described below.

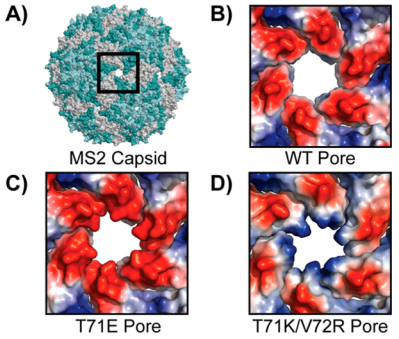

Figure 2. Vacuum electrostatic representations of pore mutants modeled in PyMOL. Negative potential is represented by red shading, and positive, by blue. (A) The capsid features ∼1.8 nm pores at each of its 5-fold or quasi-6-fold axes. (B) Wild-type MS2 has negative charge around the pore periphery but not inside. (C) Mutant T71E has significant negative charge throughout the pore. (D) Mutant T71K/V72R has positive charge in the pore.

To ensure complete encapsulation of $PhoA^{WT}$-neg, the enzyme was labeled with fluorescein 5(6)-isothiocyanate (FITC). The labeling had no effect on the enzymatic activity (Supporting Information Figure S4). The labeled enzyme was encapsulated in each of the capsid mutants. Upon encapsulation, a change in optical properties of the dye was observed; therefore, fluorescein was used only as a qualitative indicator of presence of the enzyme within the capsid. Enzyme quantification was performed by running the purified capsid constructs on SDS-PAGE gels followed by Coomassie staining and optical densitometry. The capsids each contained a similar amount of enzyme, with the $MS2^{WT}$ and $MS2^{T71K/V72R}$ capsids carrying slightly more, followed by the $MS2^{T71E}$ then $MS2^{T71E/V72D}$ capsids (Supporting Information Table S2). It is not surprising that added negative charge decreases the amount of encapsulated enzyme due to the electrostatic nature of the interaction between $PhoA^{WT}$-neg and the capsid. We also found that increasing the salt concentration lowered the number of enzymes encapsulated per $MS2^{WT}$ capsid (Supporting Information Figure S5), supporting the importance of electrostatics in the enzyme/capsid interaction during assembly. Moreover, $MS2^{WT}$ capsids with varying numbers of enzymes encapsulated showed indistinguishable $k_{cat,app}$ and $K_{M,app}$ kinetic parameters, as expected (Figure 3).

Capsid Mutations Impact Kinetics of Encapsulated PhoA. We evaluated the Michaelis−Menten kinetics of the hydrolysis of 4-methylumbelliferyl phosphate to 4-methylumbelliferone catalyzed by $PhoA^{WT}$-neg in each of the capsids, as shown in Figure 4A. We chose to do the experiments in low-concentration Tris buffer, although similar trends were observed in MOPS (Supporting Information Table S3). Although the presence of Tris can lead to transphosphorylation onto the buffer, artificially increasing k_{cat}, this effect is negligible

DOI: 10.1021/acssynbio.5b00037
ACS Synth. Biol. 2015, 4, 1011−1019

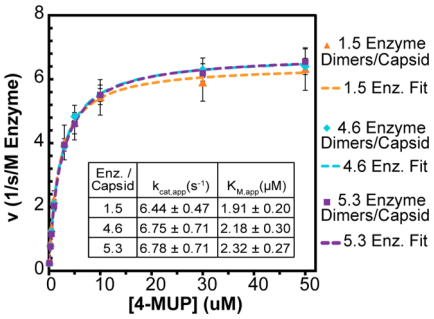

Figure 3. Enzyme assays with PhoA^{WT}-neg encapsulated into MS2^{WT} at different levels of enzyme loading. Error bars represent standard deviation of three assays for three separate encapsulations each. The inset displays calculated Michaelis–Menten parameters $K_{M,app}$ and $k_{cat,app}$, which were found to be not significantly different among the three loading levels.

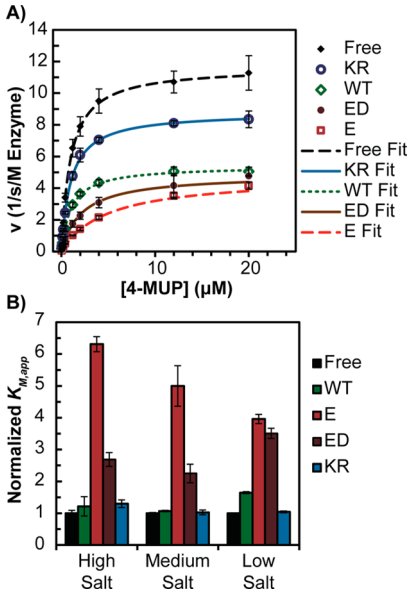

Figure 4. Enzyme assays with free and encapsulated PhoA^{WT}-neg. (A) Michaelis–Menten curves of the enzyme encapsulated in each MS2 pore variant in 10 mM Tris, pH 8.0, 100 mM NaCl (medium salt). (B) Apparent K_M of the enzyme in each pore variant in 10 mM Tris, pH 8.0, with 4 mM (low salt), 100 mM (medium salt), or 500 mM NaCl (high salt). The $K_{M,app}$ of both negative pore mutants, E and ED, increases significantly. Each $K_{M,app}$ was normalized to the free enzyme in the corresponding buffer conditions. Error bars represent standard deviation of three assays.

at the low concentrations used here (10 mM).[43] At the pH of the reaction, both the substrate and the product are negatively charged, which could lead to electrostatic effects on flux both into and out of the compartment.

As we observed previously, the MS2^{WT} capsid had no effect on the apparent K_M ($K_{M,app}$) but a modest inhibitory effect on the k_{cat}. Interestingly, encapsulation in the MS2$^{T71K/V72R}$ capsid had little effect on the $K_{M,app}$ and a less inhibitory effect on the k_{cat} than encapsulation within MS2^{WT}. On the contrary, both the negative pore mutants significantly increased the $K_{M,app}$ of the reaction while decreasing the overall k_{cat}. The increase in $K_{M,app}$ persists at a variety of salt concentrations (Figure 4B). Theoretical studies suggest electrostatic barriers in nanopores can be overcome by high ionic strength even when the substrate size approaches the Debye length of the pore.[44] Our pores are much smaller than previously studied channels, and our data suggest that our system is not in this regime, even at 0.5 M NaCl.[45] The Debye length under this condition is 0.43 nm compared to a substrate radius of approximately 0.3 nm and a pore radius of 0.9 nm.

Curiously, encapsulation in the MS2^{T71E} capsid increased the $K_{M,app}$ significantly more than encapsulation within the MS2$^{T71E/V72D}$ capsid. It is possible that the double mutation changed the pore diameter or electrostatic environment through electrostatic repulsion or other steric effects. We note that we did not directly measure the electrostatic landscape of the mutated pores, and quantification of the level of negative charge around the pore is difficult. Our results suggest that two mutations in the MS2$^{T71E/V72D}$ capsid may cause changes in the pore environment to form an electrostatic barrier similar to that of the MS2^{T71E} capsid.

In order to extend our exploration of the effects of encapsulation, we next examined a mutant of alkaline phosphatase that has different kinetic parameters. This mutant, D153G/D330N (PhoA$^{D153G/D330N}$-neg), was developed to have significantly higher values of k_{cat} and K_M while suffering less inhibition from free phosphate.[46] We speculated that product inhibition by free phosphate was affecting the kinetic behavior observed in the various capsids, and this enzyme permitted further investigation of this effect. We expressed the PhoA$^{D153G/D330N}$-neg mutant and encapsulated it in MS2^{WT} and MS2^{T71E} capsids. The kinetics of the free PhoA$^{D153G/D330N}$-neg enzyme, as expected, showed an increase in both $k_{cat,app}$ and $K_{M,app}$ relative to those of the free wild-type enzyme (Supporting Information Table S3). When encapsulated in MS2^{WT} capsid, this enzyme had a moderate increase in $K_{M,app}$; encapsulation in the MS2^{T71E} capsid led to an even more pronounced increase in the $K_{M,app}$, suggesting that charge repulsion remains important with the mutant enzyme.

We hypothesized that the MS2^{T71E} capsid pores could inhibit the transport of negatively charged species more than those of the MS2^{WT} capsid, resulting in increased inhibitory effects on k_{cat} and $K_{M,app}$. Direct measurements of the phosphate ion concentration inside the capsid relative to the assay bulk were impractical, so we pursued a modeling strategy to demonstrate the feasibility of this ion-trapping mechanism. The kinetic behavior of the MS2/PhoA-neg nanoreactor system is different from the case of the free enzyme due to the effects both of small molecule transport and of enzyme immobilization on kinetic behavior. Since we could not determine the quantitative effects of immobilization, we developed a model based on the enzyme kinetic parameters observed for alkaline phosphatase within the MS2^{WT} capsid and attempted to describe the altered kinetics of the MS2^{T71E} encapsidated enzyme solely by altering transport parameters.

Modeling Suggests a Role for Phosphate Transport in Kinetic Differences. The MS2 nanoreactor was modeled using the reaction scheme shown in Figure 5A, treating the MS2 capsid interior and the assay bulk as two distinct, well-mixed phases. The model incorporates substrate diffusion between the bulk and the capsid, as represented by the permeability parameter k_1, classical Michaelis–Menten enzyme kinetics with competitive product inhibition by phosphate,[47] and phosphate diffusion out of the capsid, as represented by the first-order rate constant k_2. We regarded the phosphate concentration in the bulk as essentially zero over the time scale modeled due to the large assay volume relative to the volume of the capsid phase. The intrinsic Michaelis–Menten

DOI: 10.1021/acssynbio.5b00037
ACS Synth. Biol. 2015, 4, 1011–1019

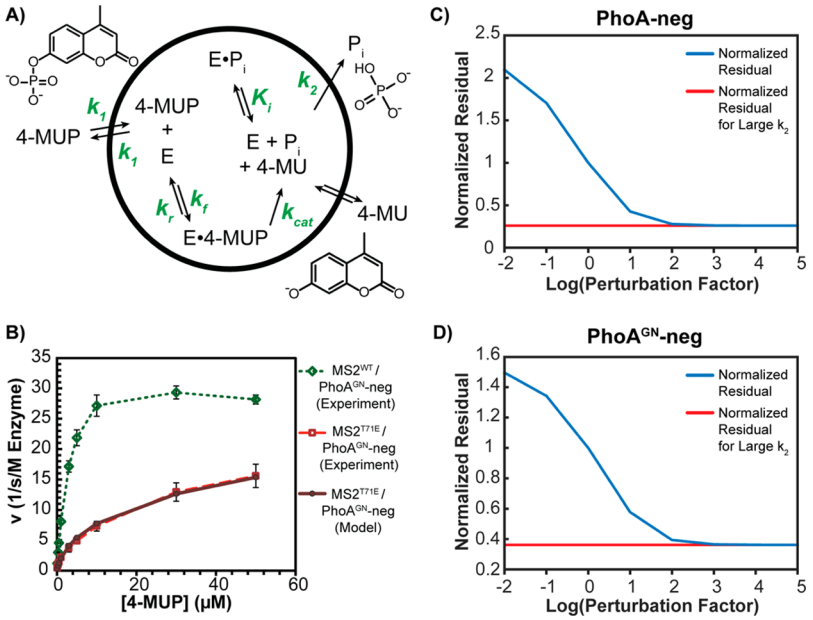

Figure 5. Kinetic model of encapsulated reactions. (A) System of reactions used as parameters for the kinetic model. Variables highlighted in green define the kinetics of the system. (B) Results of the model for encapsulated PhoA$^{D153G/D330N}$-neg. (C) Relaxation of parameter k_2 to approximate MS2^{WT} behavior for encapsulated PhoA^{WT}-neg. The blue line represents the residual between the MS2^{WT} experimental data and the best fit to the MS2^{T71E} case, normalized to the residual at the fitted k_2 value, plotted as the fitted value of k_2 multiplied by a perturbation factor ranging from 0.001 to 1000. The red line represents the minimum residual value in the limit of large k_2. (D) The same calculation as (C), performed for encapsulated PhoA$^{D153G/D330N}$-neg.

parameters $k_{cat,app}$ and $K_{M,app}$ for the PhoA^{WT}-neg and PhoA$^{D153G/D330N}$-neg enzymes, as fitted to the MS2^{WT} capsid case, were held constant in the MS2^{T71E} capsid case for each enzyme, as we assume that the intrinsic kinetic properties of the encapsulated enzymes differed from the free enzyme but are not altered by the capsid mutations.[48] Experimental results and fitted models are shown in Figure 5B.

The transport parameters k_1 and k_2 capture the effects of the T71E pore mutation on substrate and inhibitor transport, respectively, relative to that of MS2^{WT} capsid (not relative to the free enzyme). The two competitive inhibition parameters, $K_{I,PhoA(WT)}$ and $K_{I,PhoA(D153G/D330N)}$, capture phosphate inhibition of the PhoA^{WT}-neg enzyme and the PhoA$^{D153G/D330N}$-neg mutant. The modeled enzyme kinetics for the PhoA$^{D153G/D330N}$-neg enzyme in the MS2^{T71E} capsid are shown alongside the MS2^{WT} and MS2^{T71E} experimental data in Figure 5B. $K_{I,PhoA(WT)}$ and $K_{I,PhoA(D153G/D330N)}$ were fitted as 1.74 and 2.67 μM, respectively. These values are comparable to the experimentally determined values of 1.4 and 6.4 μM (Supporting Information Figure S6) found in the case of free enzyme inhibition by phosphate, validating the applicability of this modeling approach. Simulated concentration profiles for the product, substrate, and competitive inhibitor are shown for each experimental substrate concentration in Supporting Information Figure S7. Product concentrations are shown normalized to the concentration of enzyme, for comparison with experiment; the substrate and inhibitor concentrations shown are those for the capsid interior phase. Both the substrate and inhibitor concentrations in the capsid are observed to reach a steady state within the first few seconds of the simulation.

The transport parameters k_1 and k_2 and the competitive inhibition constants K_I fitted for the PhoA^{WT}-neg case and for the case using the PhoA$^{D153G/D330N}$-neg enzyme are shown in Table 1. By considering the geometry of the capsids, the phosphate transport parameter k_2 can be reinterpreted as an apparent diffusion coefficient for transport from the capsid interior across the pores of the capsid shell into the assay bulk (Table 1; see Supporting Information for calculation). We note that this conversion is dependent on many physical parameters that are not known with certainty; the apparent diffusivity should therefore be regarded as an estimate. The apparent diffusivity calculated in this way is much smaller than the diffusion coefficient of free phosphate in water (5×10^{-6} cm^2/s). It is possible that there are significant Coulombic effects on the diffusion of charged species through the pores, since the radius of the pores of the MS2 capsid is on the same order of magnitude as the Debye length of the system. Therefore, these lower apparent diffusivities are not unreasonable and might be expected to be modulated by the amino acid character of the residues surrounding the pore, as we observe.

Table 1. Fitted Parameters from Kinetic Model and Calculated Apparent Diffusivity D_2

parameter	fitted value
k_1 (1/s)	$\geq 1.02 \times 10^4$
k_2 (1/s)	6.08×10^2
D_2 (cm^2/s)	1.64×10^{-9}
$K_{I(WT)}$ (μM)	1.74
$K_{I(GN)}$ (μM)	2.67

We assessed the numerical uncertainty associated with each fitted parameter by calculating the residual error between the model and the experimental data for a range of values for each fitted parameter. A more rapid increase in the residual as the parameter value moves away from its fitted value indicates lower uncertainty in its estimated value from fitting. Plots of the residual error for perturbations in each parameter for the PhoA^{WT}-neg and the PhoA$^{D153G/D330N}$-neg cases can be found in Supporting Information Figure S8. In particular, we find that

DOI: 10.1021/acssynbio.5b00037
ACS Synth. Biol. 2015, 4, 1011−1019

the fitted value of k_1 represents, at best, a lower bound on its value: the residual error is not observed to increase significantly even with large increases in the value of k_1. The intracapsid substrate concentration was observed to rapidly equilibrate with the substrate concentration in the bulk due to the small volume of the capsid phase relative to the assay bulk; increases in the substrate transport parameter k_1, therefore, have little effect on the steady-state substrate concentration encountered by encapsulated enzymes. Due to this numerical uncertainty, we did not attempt to interpret this parameter as an apparent diffusivity. The phosphate escape parameter k_2, on the other hand, has a strong impact on the steady-state inhibitor concentration in the capsid and hence the enzymatic rate.

In order to test whether our model could describe the behavior of both the $MS2^{WT}$ and $MS2^{T71E}$ systems, we estimated the change in k_2 required to recapitulate the behavior of the $MS2^{WT}$ system by computing the residual error between the model and the $MS2^{WT}$ experimental data as a function of the value of k_2, beginning with the value found by fitting to the $MS2^{T71E}$ experimental data (Supporting Information Figure S8). Since the intrinsic enzyme parameters were initially fitted to the $MS2^{WT}$ system, the model will approximate the $MS2^{WT}$ system in the limit of very high k_2 (no transport limitation). We find that, in the case of the $PhoA^{WT}$-neg enzyme, the residual approaches its limiting value upon a 100-fold increase in k_2 and upon a 100- to 1000-fold increase in k_2 for the $PhoA^{D153G/D330N}$-neg case. Thus, changes in k_2 alone, as might be caused by the amino acid mutation T71E in the MS2 capsid, are sufficient to describe the behavior of both systems in our model.

In addition to the assumption of two well-mixed phases and the assumption that the intrinsic kinetics of an enzyme in the $MS2^{WT}$ capsid are unaffected by the T71E pore mutation, the model accounts neither for modes of inhibition other than product inhibition by phosphate nor for variations in the amount of enzyme loaded in each individual capsid in a sample. Despite these simplifications, we find that our model, in which substrate and inhibitor diffusion through the pore are inhibited in the negatively charged $MS2^{T71E}$ pore relative to $MS2^{WT}$, can account for the decrease in $k_{cat,app}$ observed in the $MS2^{T71E}$ capsid as well as the increase in $K_{M,app}$, for both $PhoA^{WT}$-neg and $PhoA^{D153G/D330N}$-neg. Typically, competitive inhibition in a Michaelis–Menten reaction scheme increases the $K_{M,app}$ but does not affect $k_{cat,app}$; in this case, however, trapping of the phosphate ion leads to increased inhibitor concentrations at higher rates of reaction (Supporting Information Figure S7), causing a decrease in the observed $k_{cat,app}$. The results of this highly simplified model are consistent with the hypothesis that changes in pore charge can affect transport into and out of the nanoreactor and thus affect observed enzyme kinetics.

Conclusions. Here, we show that a porous capsid-based nanocompartment can be modified to have specific effects on encapsulated enzymatic reactions by regulating substrate and product transport into and out of the system. We expect this type of transport control to be especially relevant in the development of multienzyme systems, where local substrate concentrations are important to enzymatic rates. In our model system, a large negatively charged substrate must overcome a Coulombic barrier to reach the enzyme. Similarly, the product must overcome a barrier to escape, potentially leading to product inhibition of the enzyme. It is important to note that this system cannot enhance the enzymatic rate; we instead demonstrate the potential of both controlled access to the interior of a protein compartment and product build up. If the system is expanded to the study of compartmentalization of a multienzyme pathway, this effect could be useful to increasing local concentration of intermediates. Increased local intermediate concentration may alleviate bottlenecks in compartmentalized metabolons caused by rate-limiting downstream enzymes. This is a key advantage in the enhancement of flux through synthetic enzymatic pathways. In the future, this study can be used to develop computational models for other designed compartments with selectivity based on size, charge, or hydrophobicity. Theories generated can then be applied to systems such as bacterial microcompartments for the production of fuels, chemical feedstocks, and pharmaceuticals in bacterial hosts.

METHODS

Reagents. Unless otherwise noted, reagents were used as received from commercial sources. In all experiments, water was deionized using a Milli-Q system (Millipore). Chemicals were obtained from Fisher Chemical except Tris base (VWR), TMAO dihydrate (Alpha Aesar), triethanolamine (Sigma), 4-methylumbelliferyl phosphate (Invitrogen), and 4-methylumbelliferone (Sigma). Molecular biology reagents were obtained from New England Biolabs.

High-Performance Liquid Chromatography. HPLC was performed using an Agilent 1100 series HPLC using ST buffer (50 mM Tris, pH 7.2, 100 mM NaCl) or sodium phosphate buffer (10 mM, pH 7.2) as mobile phase. All size exclusion chromatography was performed using a Biosep SEC-4000 column (Phenomenex). Liquid chromatography/mass spectrometry (LC/MS) was performed using an Agilent 1200 series HPLC connected to an Agilent 6224 time-of-flight (TOF) LC/MS system equipped with a turbospray ion source. For purification, samples were filtered through 0.22 μm filters (Millipore). HPLC-based quantification was performed by comparing integrated fluorescence intensity of tryptophan (λ_{ex} 280/λ_{em} 330) over time of untreated MS2 to reassembled samples.

Dynamic Light Scattering. DLS was performed using a Zetasizer Nano (Malvern Instruments). Before analysis, samples were filtered through 0.22 μm filters (Millipore). Measurements were taken in 50 mM Tris, pH 7.2, 100 mM NaCl.

Enzyme Kinetics. Enzyme assays were performed in 96-well plates 10 wells at a time. Fluorescence was read using a Spectramax M2 plate reader (Molecular Devices). The excitation wavelength was 360 nm, and the emission wavelength was 449 nm. Substrate stock solutions of 4-methylumbelliferyl phosphate and standards of 4-methylumbelliferone were prepared fresh daily to account for background substrate hydrolysis, bleaching, or variability in plate reader signal. Michaelis–Menten parameters were determined by fitting to the Michaelis–Menten equation in OriginPro 8 and R software.

Gel Analyses. Sodium dodecyl sulfate polyacrylamide gel electrophoresis (SDS-PAGE) analysis of all protein samples was carried out on a Mini Protean apparatus (Bio-Rad, Hercules, CA) using 12.5% polyacrylamide gels prepared according to the manufacturer's specifications. Samples were heated at 95 °C in the presence of Laemmli buffer containing β-mercaptoethanol for 3 to 5 min. Gels were run at 125 V for approximately 75 min, stained with Coomassie R-250, and imaged using a Chemidoc imager (Bio-Rad). Molecular masses

DOI: 10.1021/acssynbio.5b00037
ACS Synth. Biol. 2015, 4, 1011–1019

were estimated by comparison to the EZ-run Prestained Rec protein ladder (Fisher). Quantification of PhoA-neg bands was accomplished by densitometry using the Chemidoc software using known quantities of free enzyme as standards.

UV−Vis Spectroscopy. UV−vis spectroscopy was performed using a Nanodrop 2000C (Thermo Scientific). Free enzyme was quantified by absorbance at 280 using an extinction coefficient of ε = 0.71 cm·mL/mg. Nucleic acid-free MS2 was quantified using ε = 1 cm·mL/mg.

Transmission Electron Microscopy. TEM images were taken using an FEI Technai 12 transmission electron microscope with an accelerating voltage of 120 kV. Samples were desalted using NAP-5 desalting columns (GE Healthcare), concentrated to approximately 50 μM using 100 kDa MWCO spin filters (Millipore), incubated on Formvar-coated copper mesh grids for 5 min, wicked off using filter paper, and dried in air briefly. These grids were then quickly washed with water and immediately wicked again. The samples were stained with 1% $UO_2(OAc)_2$ for 2 min and again wicked and dried.

Generation of MS2 Mutants. The residues around the pore of the capsid, specifically T71 and V72 (numbering based on PDB crystal structure 1ZDK), were targeted for mutation using the QuikChange method. The mutagenesis primers were found to interfere with ColE1 plasmid origins, so the gene for wild-type MS2 was cloned into pBAD33 with a p15A origin. The gene for wild-type MS2 coat protein was PCR-amplified from pBAD-*myc-his*-WTMS2, retaining that construct's 5′ XbaI and 3′ HindIII sites (forward: 5′-AGTCAGCCGTTTTCTAGACTAACAGG-3′; reverse: 5′-AGTCAGCCCAAGCTTAGTAGATGCCG-3′). The gene was digested, ligated into pBAD33, and transformed into DH10B cells.

Plasmid pBAD33-WTMS2 was used to generate mutants T71E, T71E/V72D, and T71K/V72R using the primers in Supporting Information Table S1. For optimal expression, the mutant genes were cloned into pTrc99a using the same method as that outlined above.

Expression and Purification of MS2. Wild-type MS2 capsid and pore variants were expressed and purified as previously described.[39] Plasmid pBAD-*myc-his* containing the gene for the wild-type capsid or pTrc99a containing the desired pore MS2 variant was transformed into DH10B cells and plated on LB + 50 mg/L carbenicillin (Cb). A single colony was grown overnight in 5 mL of LB + Cb and used to inoculate 500 mL of 2×YT + Cb at a 1:500 dilution. This culture was shaken at 37 °C until it reached an OD_{600} of 0.5, at which time it was induced with 0.2% arabinose (for pBAD) or 1 mM IPTG (for pTrc) and allowed to express overnight at the same temperature.

Cells were harvested, resuspended in 10 mM taurine, pH 9.0, and lysed by sonication. The clarified lysate was applied to a DEAE column, and the flowthrough containing the MS2 mutant was retained. To precipitate the capsid, solid poly(ethylene glycol) 8k, and 5 M NaCl were added to final concentrations of 10% w/v and 0.5 M, respectively, and the mixture was incubated at 4 °C for 1 h on an orbital shaker and centrifuged at 14 000*g* for 30 min. The pelleted protein was resuspended in a small amount of 10 mM phosphate buffer, pH 7.2, and centrifuged again. The resolubilized capsid was then applied to a S200 size exclusion chromatography column and eluted in 10 mM phosphate buffer. Fractions containing MS2 were reprecipitated and stored at 4 °C.

Generation of PhoA^{WT}-neg and PhoA$^{D153G/D330N}$-neg. The *phoA* gene was amplified from *E. coli* DH10B genomic DNA, inserted into a pTrc99a vector, reamplified with PCR primers to add a C-terminal sequence of EEEEDDDEDDDDEEDD (forward primer 5′-ACACTGTCTAGAGTGAAACAAAGCACTATTGCAC-3′, reverse primer 5′-ACACTGAAGCTTTTAATCGTCTTCCTCGTCATCGTCATCTTCGTCATCATCCTCTTCTTCCTCTTTCAGCCCCAGAGCG), and reinserted into pTrc99a. To generate PhoA$^{D153G/D330N}$-neg, plasmid pTrc99a harboring the gene for PhoA^{WT}-neg was subjected to two successive rounds of QuikChange mutagenesis. First, the D330N mutation was made using forward primer 5′-GTGCGTCAATCGATAAACAGAATCATGCTGCGAATCCTTG-3′ and reverse primer 5′-CAAGGATTCGCAGCATGATTCTGTTTATCGATTGACGCAC-3′, and the resulting plasmid was transformed into DH10B cells, isolated, and sequenced. The D153G mutation was then made using forward primer 5′-CGTTTCTACCGCAGAGTTGCAGGGCGCCACGCCCGCTGCGCTGGTGGC-3′ and reverse primer 5′-GCCACCAGCGCAGCGGGCGTGGCGCCCTGCAACTCTGCGGTAGAAACG-3′, and resulting plasmids were again transformed into DH10B cells, isolated, and sequenced.

Expression and Purification of PhoA^{WT}-neg and PhoA$^{D153G/D330N}$-neg. PhoA^{WT}-neg and PhoA$^{D153G/D330N}$-neg were expressed and purified as previously described.[39] Plasmid pTrc99a harboring the gene for the desired enzyme was transformed into DH1 cells and plated on LB-Cb. A single colony was grown overnight in 5 mL of LB + Cb and used to inoculate 1 L of 2×YT + Cb supplemented with 1 mM $MgSO_4$ and 0.1 mM $ZnSO_4$ at a 1:500 dilution. This culture was shaken at 37 °C until it reached an OD_{600} of 0.5, at which time it was induced with 1 mM IPTG and allowed to express overnight at the same temperature.

Cells were harvested and washed once with 100 mL of 50 mM Tris HCl, pH 8.0, and resuspended in 50 mL of the Tris buffer. Periplasmic proteins were isolated by addition of solid sucrose to 500 mM, 500 mM EDTA to 2.5 mM, and lysozyme to 0.6 mg/mL. The resulting suspension was gently mixed and incubated at 37 °C for 30 min, followed by centrifugation at 5000*g* for 20 min. Solutions of $MgSO_4$ and $ZnSO_4$ were added to 10 and 1 mM final concentrations, respectively, and the mixture was heated at 80 °C for 10 min, with intermittent mixing. Precipitated protein was pelleted by centrifugation at 10 000*g* for 20 min followed by filtration through a 0.22 μm filter. This was then applied to a 5 mL bed of DEAE-sepharose and washed with 20 mL aliquots of 20 mM Tris containing 0, 50, and 100 mM NaCl. The protein was eluted with 250 mM NaCl and stored at 4 °C in the same buffer with $MgSO_4$ and $ZnSO_4$ added to 1 and 0.1 mM final concentrations, respectively. This protocol yields approximately 40 mg of PhoA^{WT}-neg and 25 mg of PhoA$^{D153G/D330N}$-neg per liter of culture.

FITC Labeling of PhoA^{WT}-neg. PhoA^{WT}-neg was dialyzed into triethanolamine buffer, pH 8.3, for labeling. Fluorescein 5(6)-isothiocyanate (50 mM freshly dissolved in DMF) was added to 1.3 mg/mL enzyme in 50-fold molar excess and incubated at 4 °C overnight. Excess FITC was removed by dialysis using a 10 kDa MWCO dialysis cassette (Pierce). Attachment of the fluorophore was confirmed by electrospray ionization-time-of-flight mass spectrometry and size exclusion chromatography using a Biosep-SEC-4000 column at a flow rate of 1 mL/min.

Encapsulation of Enzymes in MS2 Mutants. A modified protocol was used to encapsulate enzymes inside MS2 pore

DOI: 10.1021/acssynbio.5b00037
ACS Synth. Biol. 2015, 4, 1011−1019

mutants. MS2 was disassembled in 66% acetic acid and desalted into 1 mM acetic acid as described. The coat protein was added to a chilled solution of enzyme (0.1 mg/mL), Bis-Tris buffer (50 mM, pH 6.0), and TMAO (1.8 M). Ionic strength was altered with the addition of varying amounts of (5.0 M) NaCl to the reassembly reaction. The capsid was allowed to reassemble for 48 h at 4 °C before purification and analysis.

Purification of Encapsulated Enzymes. Reassembled capsid containing the desired enzyme derivative was purified by precipitation with PEG 8k followed by SEC-HPLC. Solid PEG 8k and 5 M NaCl were added to the reassembly reaction to a final concentrations of 10% and 0.5 M, respectively, and the mixture was incubated at 4 °C on an orbital shaker and centrifuged at 21 000*g* for 10 min. The precipitated capsids were resuspended in ST buffer (50 mM Tris, pH 7.2, 100 mM NaCl) and centrifuged again to pellet any aggregated protein. The supernatant was filtered through a 0.22 μm filter and injected on a Biosep-SEC-4000 column. ST buffer was pumped over the column at 1 mL/min, and reassembled MS2, which elutes at ∼6.3 min, was collected and concentrated using 100 kDa MWCO centrifugal filters (Millipore).

Evaluation of Stability of MS2-Encapsulated PhoA^{WT}-neg. We examined thermal stability of our system using dynamic light scattering (DLS). Size trends upon change in temperature were recorded for each capsid, starting at 35 °C, in 4 °C steps with a 5 min incubation at each temperature.

Enzyme Kinetics. Kinetics of free and encapsulated enzymes were measured by monitoring the increase in fluorescence (λ_{ex} 360 nm/λ_{em} 449 nm) upon hydrolysis of the phosphoester bond in 4-methyl-umbelliferyl phosphate. The enzyme (100 μL, 2 nM monomer) in 2× buffer was added to the 100 μL H_2O containing the substrate at increasing concentrations, and initial rates were recorded. Standards of 4-methylumbelliferone were used to generate a standard curve in the relevant signal range to convert fluorescent signal to concentration. Data were fit to the Michaelis−Menten equation using OriginPro 8 or R fitting software. Assays were done in the following buffers: 50 mM MOPS, pH 8.0, 500 mM NaCl, 1 mM $MgSO_4$, 0.1 mM $ZnSO_4$ (high salt); 50 mM MOPS, pH 8.0, 1 mM $MgSO_4$, 0.1 mM $ZnSO_4$ (low salt); 10 mM Tris, pH 8.0, 4 mM NaCl, 1 mM $MgSO_4$, 0.1 mM $ZnSO_4$ (low salt); 10 mM Tris, pH 8.0, 100 mM NaCl, 1 mM $MgSO_4$, 0.1 mM $ZnSO_4$ (medium salt); 10 mM Tris, pH 8.0, 500 mM NaCl, 1 mM $MgSO_4$, 0.1 mM $ZnSO_4$ (high salt).

Experimental Determination of Inhibition Constants (K_I) for Free Enzymes. Free PhoA^{WT}-neg and PhoA$^{D153G/D330N}$-neg were incubated with increasing concentrations of phosphate and assayed in medium salt buffer for kinetic parameters as described above. The resulting $K_{M,app}$ values were plotted against phosphate concentrations and fit to the K_I equation.

Nanoreactor Kinetics Modeling. Modeling of kinetic parameters was performed in MATLAB using the reaction scheme shown in Figure 5A. The model incorporated substrate diffusion between the bulk and the capsid (k_1), Michaelis−Menten enzyme kinetics (k_{cat}) with competitive product inhibition by phosphate (K_I), and phosphate diffusion out of the capsid, as represented by the first-order rate constant k_2. Kinetic studies of the PhoA^{WT}-neg and PhoA$^{D153G/D330N}$-neg enzymes in the MS2^{T71E} capsid were simulated by numerical integration of the reaction scheme for each substrate concentration tested experimentally, producing a plot of product concentration against time for each substrate concentration (Supporting Information Figure S7). A linear regression was then used to fit the initial reaction rate for comparison to the experimental data (Supporting Information Figure S7). The model thus generates a set of rates of product formation as a function of substrate concentration. The four kinetic parameters (k_1, k_2, $K_{I,PhoA(WT)}$, and $K_{I,PhoA(D153G/D330N)}$) were then fitted to the experimental data for both the PhoA^{WT}-neg and PhoA$^{D153G/D330N}$-neg enzymes simultaneously by minimization of the sum of the square errors between the simulated data and the data from experiment, using the built-in lsqnonlin minimization function in MATLAB.

■ ASSOCIATED CONTENT

Supporting Information

Calculations and description of the model. Figure S1: Reassembly of capsid mutants around PhoA^{WT}-neg. Figure S2: Structure and stability of MS2-encapsulated PhoA^{WT}-neg derivatives. Figure S3: Kinetics of free PhoA^{WT}-neg in medium and low salt Tris buffer after treatment with reassembly and purification conditions. Figure S4: Analysis of kinetics of FITC-labeled and unlabeled PhoA^{WT}-neg in high salt MOPS. Figure S5: Loading of PhoA^{WT}-neg in MS2^{WT} varies inversely with the ionic strength of the reassembly reaction. Figure S6: Experimental determination of K_I for free PhoA^{WT}-neg and PhoA$^{D153G/D330N}$ in medium salt Tris buffer. Figure S7: Simulated concentration profiles for the product, substrate, and competitive inhibitor for each experimental substrate concentration for the PhoA^{WT}-neg and PhoA$^{D153G/D330N}$ cases. Figure S8: Sensitivity analysis for kinetics parameters. Table S1: Mutagenesis primers for MS2 capsid pore mutants. Table S2: Enzyme loading in MS2 derivatives. Table S3: Kinetic constants for free and encapsulated PhoA^{WT}-neg and PhoA$^{D153G/D330N}$-neg derivatives under several conditions. The Supporting Information is available free of charge on the ACS Publications website at DOI: 10.1021/acssynbio.5b00037.

■ AUTHOR INFORMATION

Corresponding Author

*E-mail: dtercek@berkeley.edu.

Author Contributions

J.E.G, D.T-E., and M.B.F. designed the project. J.E.G. and M.A.A performed the experiments, and C.M.J. created the mathematical model. J.E.G., M.A.A, C.M.J, and D.T.-E. wrote the manuscript.

Notes

The authors declare no competing financial interest.

■ ACKNOWLEDGMENTS

The authors wish to thank the Matthew Francis and Michelle Chang laboratories for helpful discussions and equipment usage as well as the Robert D. Ogg Electron Microscope Laboratory for equipment usage and training. The authors would also like to thank the Tullman-Ercek lab for insightful comments. The work was funded by the Hellman Family Faculty Fund (J.E.G.) and the National Science Foundation (award MCB1150567 to C.M.J. and D.T.-E.).

■ REFERENCES

(1) Huang, X., Holden, H. M., and Raushel, F. M. (2001) Channeling of substrates and intermediates in enzyme-catalyzed reactions. *Annu. Rev. Biochem. 70*, 149−180.

DOI: 10.1021/acssynbio.5b00037
ACS Synth. Biol. 2015, 4, 1011−1019

(2) Jandt, U., You, C., Zhang, Y. H.-P., and Zeng, A.-P. (2013) Compartmentalization and metabolic channeling for multienzymatic biosynthesis: practical strategies and modeling approaches, in *Fundamentals and Application of New Bioproduction Systems* (Zeng, A.-P., Ed.) pp 1−25, Springer, Heidelberg.
(3) Zhang, Y.-H. P. (2011) Substrate channeling and enzyme complexes for biotechnological applications. *Biotechnol. Adv. 29*, 715−725.
(4) Agapakis, C. M., Boyle, P. M., and Silver, P. A. (2012) Natural strategies for the spatial optimization of metabolism in synthetic biology. *Nat. Chem. Biol. 8*, 527−535.
(5) Idan, O., and Hess, H. (2013) The origins of activity enhancement in enzyme cascades on scaffolds. *ACS Nano 7*, 8658−8665.
(6) Conrado, R. J., Varner, J. D., and DeLisa, M. P. (2008) Engineering the spatial organization of metabolic enzymes: mimicking nature's synergy. *Curr. Opin. Biotechnol. 19*, 492−499.
(7) Ovádi, J., and Srere, P. A. (1999) Macromolecular compartmentation and channeling, in *International Review of Cytology* (Walter, H., Brooks, D., and Srere, P., Ed.) pp 255−280, Academic Press, New York.
(8) Conrado, R. J., Mansell, T. J., Varner, J. D., and DeLisa, M. P. (2007) Stochastic reaction−diffusion simulation of enzyme compartmentalization reveals improved catalytic efficiency for a synthetic metabolic pathway. *Metab. Eng. 9*, 355−363.
(9) Conrado, R. J., Wu, G. C., Boock, J. T., Xu, H., Chen, S. Y., Lebar, T., Turn\vsek, J., Tom\vsi\vc, N., Avbelj, M., and Koprivnjak, T. (2012) DNA-guided assembly of biosynthetic pathways promotes improved catalytic efficiency. *Nucleic Acids Res. 40*, 1879−1889.
(10) Delebecque, C. J., Lindner, A. B., Silver, P. A., and Aldaye, F. A. (2011) Organization of intracellular reactions with rationally designed RNA assemblies. *Science 333*, 470−474.
(11) Dueber, J. E., Wu, G. C., Malmirchegini, G. R., Moon, T. S., Petzold, C. J., Ullal, A. V., Prather, K. L., and Keasling, J. D. (2009) Synthetic protein scaffolds provide modular control over metabolic flux. *Nat. Biotechnol. 27*, 753−759.
(12) Lee, H., DeLoache, W. C., and Dueber, J. E. (2012) Spatial organization of enzymes for metabolic engineering. *Metab. Eng. 14*, 242−251.
(13) Moon, T. S., Dueber, J. E., Shiue, E., and Prather, K. L. J. (2010) Use of modular, synthetic scaffolds for improved production of glucaric acid in engineered *E. coli*. *Metab. Eng. 12*, 298−305.
(14) Avalos, J. L., Fink, G. R., and Stephanopoulos, G. (2013) Compartmentalization of metabolic pathways in yeast mitochondria improves the production of branched-chain alcohols. *Nat. Biotechnol. 31*, 335−341.
(15) Heinig, U., Gutensohn, M., Dudareva, N., and Aharoni, A. (2013) The challenges of cellular compartmentalization in plant metabolic engineering. *Curr. Opin. Biotechnol. 24*, 239−246.
(16) You, C., Myung, S., and Zhang, Y.-H. P. (2012) Facilitated substrate channeling in a self-assembled trifunctional enzyme complex. *Angew. Chem., Int. Ed. 51*, 8787−8790.
(17) Torres Pazmiño, D. E., Riebel, A., de Lange, J., Rudroff, F., Mihovilovic, M. D., and Fraaije, M. W. (2009) Efficient biooxidations catalyzed by a new generation of self-sufficient Baeyer-Villiger monooxygenases. *ChemBioChem 10*, 2595−2598.
(18) You, C., and Zhang, Y.-H. P. (2014) Annexation of a high-activity enzyme in a synthetic three-enzyme complex greatly decreases the degree of substrate channeling. *ACS Synth. Biol. 3*, 380−386.
(19) Bode, S. A., Minten, I. J., Nolte, R. J. M., and Cornelissen, J. J. L. M. (2011) Reactions inside nanoscale protein cages. *Nanoscale 3*, 2376.
(20) Minten, I. J., Claessen, V. I., Blank, K., Rowan, A. E., Nolte, R. J. M., and Cornelissen, J. J. L. M. (2011) Catalytic capsids: the art of confinement. *Chem. Sci. 2*, 358.
(21) Cardinale, D., Carette, N., and Michon, T. (2012) Virus scaffolds as enzyme nano-carriers. *Trends Biotechnol. 30*, 369−376.
(22) Kim, E. Y., and Tullman-Ercek, D. (2013) Engineering nanoscale protein compartments for synthetic organelles. *Curr. Opin. Biotechnol. 24*, 627−632.
(23) Patterson, D. P., Schwarz, B., Waters, R. S., Gedeon, T., and Douglas, T. (2014) Encapsulation of an enzyme cascade within the bacteriophage P22 virus-like particle. *ACS Chem. Biol. 9*, 359−365.
(24) Broz, P., Driamov, S., Ziegler, J., Ben-Haim, N., Marsch, S., Meier, W., and Hunziker, P. (2006) Toward intelligent nanosize bioreactors: a pH-switchable, channel-equipped, functional polymer nanocontainer. *Nano Lett. 6*, 2349−2353.
(25) Siti, W., de Hoog, H.-P. M., Fischer, O., Shan, W. Y., Tomczak, N., Nallani, M., and Liedberg, B. (2014) An intercompartmental enzymatic cascade reaction in channel-equipped polymersome-in-polymersome architectures. *J. Mater. Chem. B 2*, 2733.
(26) Gaitzsch, J., Appelhans, D., Wang, L., Battaglia, G., and Voit, B. (2012) Synthetic bio-nanoreactor: mechanical and chemical control of polymersome membrane permeability. *Angew. Chem., Int. Ed. 51*, 4448−4451.
(27) Schoffelen, S., and van Hest, J. C. M. (2012) Multi-enzyme systems: bringing enzymes together in vitro. *Soft Matter 8*, 1736.
(28) van Oers, M. C. M., Rutjes, F. P. J. T., and van Hest, J. C. M. (2014) Cascade reactions in nanoreactors. *Curr. Opin. Biotechnol. 28*, 10−16.
(29) Louzao, I., and van Hest, J. C. M. (2013) Permeability effects on the efficiency of antioxidant nanoreactors. *Biomacromolecules 14*, 2364−2372.
(30) Dergunov, S. A., Durbin, J., Pattanaik, S., and Pinkhassik, E. (2014) pH-mediated catch and release of charged molecules with porous hollow nanocapsules. *J. Am. Chem. Soc. 136*, 2212−2215.
(31) Kim, K. T., Cornelissen, J. J. L. M., Nolte, R. J. M., and van Hest, J. C. M. (2009) A polymersome nanoreactor with controllable permeability induced by stimuli-responsive block copolymers. *Adv. Mater. 21*, 2787−2791.
(32) Kim, J.-K., Lee, E., Lim, Y., and Lee, M. (2008) Supramolecular capsules with gated pores from an amphiphilic rod assembly. *Angew. Chem., Int. Ed. 47*, 4662−4666.
(33) Fornasiero, F., Park, H. G., Holt, J. K., Stadermann, M., Grigoropoulos, C. P., Noy, A., and Bakajin, O. (2008) Ion exclusion by sub-2-nm carbon nanotube pores. *Proc. Natl. Acad. Sci. U.S.A. 105*, 17250−17255.
(34) Theil, E. C. (2011) Ferritin protein nanocages use ion channels, catalytic sites, and nucleation channels to manage iron/oxygen chemistry. *Curr. Opin. Chem. Biol. 15*, 304−311.
(35) Roux, B., Berneche, S., Egwolf, B., Lev, B., Noskov, S. Y., Rowley, C. N., and Yu, H. (2011) Perspectives on: Ion selectivity: ion selectivity in channels and transporters. *J. Gen. Physiol. 137*, 415−426.
(36) Yeates, T. O., Jorda, J., and Bobik, T. A. (2013) The shells of BMC-type microcompartment organelles in bacteria. *J. Mol. Microbiol. Biotechnol. 23*, 290−299.
(37) Kinney, J. N., Axen, S. D., and Kerfeld, C. A. (2011) Comparative analysis of carboxysome shell proteins. *Photosynth. Res. 109*, 21−32.
(38) Kerfeld, C. A., Sawaya, M. R., Tanaka, S., Nguyen, C. V., Phillips, M., Beeby, M., and Yeates, T. O. (2005) Protein structures forming the shell of primitive bacterial organelles. *Science 309*, 936−938.
(39) Glasgow, J. E., Capehart, S. L., Francis, M. B., and Tullman-Ercek, D. (2012) Osmolyte-mediated encapsulation of proteins inside MS2 viral capsids. *ACS Nano 6*, 8658−8664.
(40) Capehart, S. L., Coyle, M. P., Glasgow, J. E., and Francis, M. B. (2013) Controlled integration of gold nanoparticles and organic fluorophores using synthetically modified MS2 viral capsids. *J. Am. Chem. Soc. 135*, 3011−3016.
(41) Stonehouse, N. J., Valegard, K., Golmohammadi, R., van den Worm, S., Walton, C., Stockley, P. G., and Liljas, L. (1996) Crystal structures of MS2 capsids with mutations in the subunit FG loop. *J. Mol. Biol. 256*, 330−339.
(42) Axblom, C., Tars, K., Fridborg, K., Orna, L., Bundule, M., and Liljas, L. (1998) Structure of phage fr capsids with a deletion in the FG loop: implications for viral assembly. *Virology 249*, 80−88.

DOI: 10.1021/acssynbio.5b00037
ACS Synth. Biol. 2015, 4, 1011−1019

(43) Dayan, J., and Wilson, I. B. (1964) The phosphorylation of Tris by alkaline phosphatase. *Biochim. Biophys. Acta, Spec. Sect. Enzymol. Subj. 81*, 620−623.
(44) Schoch, R., Han, J., and Renaud, P. (2008) Transport phenomena in nanofluidics. *Rev. Mod. Phys. 80*, 839−883.
(45) Plecis, A., Schoch, R. B., and Renaud, P. (2005) Ionic transport phenomena in nanofluidics: experimental and theoretical study of the exclusion-enrichment effect on a chip. *Nano Lett. 5*, 1147−1155.
(46) Muller, B. H., Lamoure, C., Le Du, M.-H., Cattolico, L., Lajeunesse, E., Lemaître, F., Pearson, A., Ducancel, F., Ménez, A., and Boulain, J.-C. (2001) Improving *Escherichia coli* alkaline phosphatase efficacy by additional mutations inside and outside the catalytic pocket. *ChemBioChem 2*, 517−523.
(47) Coleman, J. E. (1992) Structure and mechanism of alkaline phosphatase. *Annu. Rev. Biophys. Biomol. Struct. 21*, 441−483.
(48) Goldstein, L. (1976) Kinetic behavior of immobilized enzyme systems. *Methods Enzymol. 44*, 397−443.

DOI: 10.1021/acssynbio.5b00037
ACS Synth. Biol. 2015, 4, 1011−1019